Bandwidth increasing mechanism by introducing a curve fixture to the cantilever generator

Weiqun Liu, Congzhi Liu, Bingyu Ren, Qiao Zhu, Guangdi Hu, and Weiqing Yang

Citation: Applied Physics Letters **109**, 043905 (2016); doi: 10.1063/1.4960147
View online: http://dx.doi.org/10.1063/1.4960147
View Table of Contents: http://scitation.aip.org/content/aip/journal/apl/109/4?ver=pdfcov
Published by the AIP Publishing

Bandwidth increasing mechanism by introducing a curve fixture to the cantilever generator

Weiqun Liu,[1,a)] Congzhi Liu,[1] Bingyu Ren,[1] Qiao Zhu,[1] Guangdi Hu,[1] and Weiqing Yang[2]
[1]*School of Mechanical Engineering, Southwest Jiaotong University, 610031 Chengdu, China*
[2]*School of Materials Science and Engineering, Southwest Jiaotong University, 610031 Chengdu, China*

(Received 8 April 2016; accepted 19 July 2016; published online 29 July 2016)

A nonlinear wideband generator architecture by clamping the cantilever beam generator with a curve fixture is proposed. Devices with different nonlinear stiffness can be obtained by properly choosing the fixture curve according to the design requirements. Three available generator types are presented and discussed for polynomial curves. Experimental investigations show that the proposed mechanism effectively extends the operation bandwidth with good power performance. Especially, the simplicity and easy feasibility allow the mechanism to be widely applied for vibration generators in different scales and environments. *Published by AIP Publishing.*
[http://dx.doi.org/10.1063/1.4960147]

Vibration energy harvesting[1] has been in the spotlight for decades due to the huge potentialities for the application of autonomous wireless sensors. Most of these generators use linear oscillators[2,3] at early stage, which efficiently operate in a narrow bandwidth required to match the excitation frequency. However, an inevitable challenge ahead is the changeability of the vibrations to be harvested. It puts forward the demand for broadband harvesters of both outperformed circuits and wideband generators,[4] especially the latter one. Enormous approaches have been proposed,[5–7] including resonance tuning,[8] multi-modal or array generators,[9,10] frequency up-conversion methods,[11] internal resonance,[12] nonlinear energy sink,[13] nonlinear generators,[14–25] etc. Among them, utilizing nonlinearities is a most common way of great interest to many researchers. Depending on the equilibrium position number, nonlinear generators can be divided into the mono-stable[14–17] or multi-stable types (bi-stable,[18–26] tri-stable[27] or more). Most of them utilize the magnetic interaction,[14,15,17–19,22] buckling,[20,21,23–26] or pre-stress[16] effects to obtain nonlinearities. Due to the relatively complex mechanisms, much work is required for modeling the structures. In some cases, the feasibility of a desired generator is limited for the difficulties to tune the pre-stress, magnetic interaction, or buckling effects precisely, especially in the MEMS scale. A simple realization is the piecewise structure[28,29] whose elastic curve is composed of two linear segments. However, the design space is restricted and thus difficult to achieve satisfying performance sometimes. In this letter, a simple nonlinear generator of using the CBCF (Cantilever Beam with a Curved Fixture) structure is presented in Fig. 1(a).

Compared with regular cantilever beams, this proposed generator uses the curve fixture with a specifically designed surface shape. When the load F increases, the beam will bend and touch the fixture's surface. Consequently, the effective length varies with the load and the tip displacement, and thus the device presents a nonlinear stiffness. With design constraints satisfied, the fixture shape curve can be arbitrarily selected for the desired nonlinear stiffness. A common choice is the polynomial

$$y(x) = a_1 x + a_2 x^2 + \cdots + a_n x^n, \tag{1}$$

in which the term a_0 is eliminated to ensure $y(0) = 0$ while the first non-zero coefficient $a_i > 0$ ($a_0 = \ldots = a_{i-1} = 0$) is required to exclude the interference of the two parts of the fixture. For simplification, we consider the case $n \leq 4$.

Considering the cantilever beam without the curve fixture, the deflection is

$$w(x) = \frac{FLx^2}{2EI} - \frac{Fx^3}{6EI}, \tag{2}$$

in which E is the Young's module, I the moment of inertia, and L the beam length. The contacting condition for the fixture and the beam is that there exists x_0 satisfying: $w(x_0) \geq y(x_0)$ with $0 < x_0 < L_F$. L_F is the fixture length.

Depending on the curves, Fig. 1(a) shows three possible types of CBCF with the example coefficients given, while Fig. 2 presents the corresponding curves $y(x)$ and their slope $y'(x)$. For easy understanding, $w(x)$ and its slope $w'(x)$ are also plotted for three different load cases.

Type 1. In this case, the beam will not touch the fixture except at $x = 0$ when the load is small. As seen in Fig. 2(a), $w(x)$ stays below $y(x)$ with a small load $F = 0.5$ N. Accompanying with the increase of F, $w(x)$ goes above $y(x)$ for a certain range starting from $x = 0$ as seen for $F = 1$ N and $F = 2.3$ N. Considering $y(0) = y'(0) = w(0) = w'(0) = 0$, the threshold F_{th} for contacting is determined by $w''(0) > y''(0)$. Then, we have $F_{th} = 2a_2 EI/L$. It can be more clearly seen in Fig. 2(b) in which the slope of $w'(x)$ and $y'(x)$ represents $w''(x)$ and $y''(x)$, respectively. $w''(x)$ is always smaller than $y''(x)$ unless F is large enough to let $w''(0) > y''(0)$. It is worth noting that the beam will always contact the fixture from $x = 0$ to the split point $S_0(x_0, y(x_0))$ tightly since $w(x)$ is above $y(x)$ over this range.

Type 2. Actually, it can be viewed as a special case of Type 1 with $a_2 = 0$ which hints $F_{th} = 0$. It means that the beam will touch the fixture as long as $F > 0$. This can be

a)Author to whom correspondence should be addressed. Electronic mail: weiqunliu@home.swjtu.edu.cn

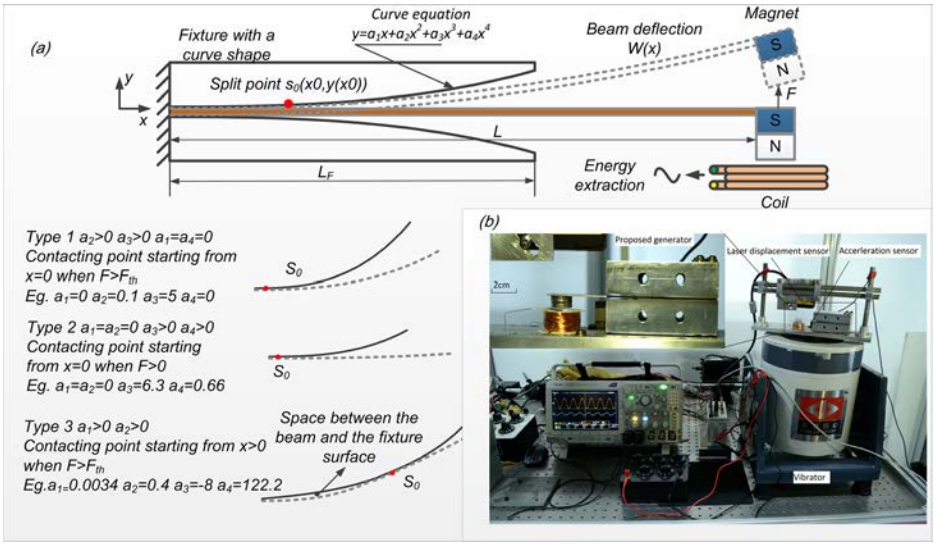

FIG. 1. (a) Scheme of the proposed CBCF nonlinear generator; (b) Experimental set-up and prototype.

well confirmed by the relationship between $y(x)$ and $w(x)$, $y'(x)$ and $w'(x)$ in Figs. 2(a) and 2(b).

Type 3. In this case, the beam will touch the fixture when F is larger than a certain threshold F_{th}. Notably, a space exists between the beam and the fixture as indicated in Fig. 1(a). It is due to the fact that the coefficient $a_1 > 0$ leads to $y'(0) = a_1 > 0$ as observed in Fig. 2(b). Considering $y(0) = w(0) = 0$, $w(x)$ and $y(x)$ can be represented by the area between $w'(x)$ and the x axis and $y'(x)$ and the x axis, respectively. Obviously, $w'(x)$ is always below $y'(x)$ around $x = 0$ with $w'(0) = 0$ and $y'(0) > 0$. Consequently, $w(x)$ stays smaller than $y(x)$ around $x = 0$ even though F is large enough to let $w(x)$ cross above $y(x)$ for a certain range as seen in Fig. 2(a). The threshold F_{th} can be calculated by the very first contacting condition.

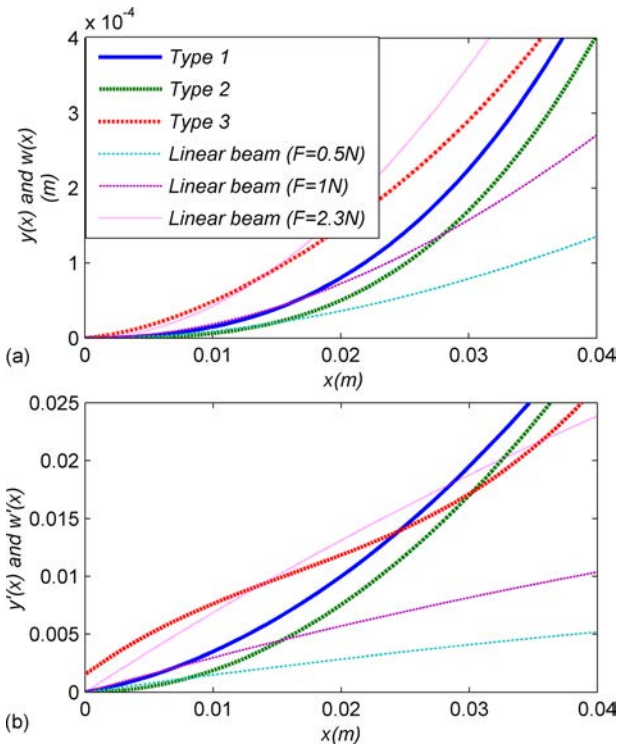

FIG. 2. Different configurations of the proposed generator and the beam deflection in different load cases: (a) the fixture curves and the beam deflection; (b) the corresponding slope.

It has to be pointed out that the beam deflection is restricted by the fixture after contacting and will not follow the trace of $w(x)$, which is accounted for the deflection without the curve fixture. Therefore, the split point S_0 cannot be determined simply by the point where $w(x)$ goes from above to below $y(x)$. Since the beam deflection is superposed with the fixture curve for the contacted area, we have the following conditions for S_0:

$$w_F(x_0) = y(x_0)\ w'_F(x_0) = y'(x_0)\ w''_F(x_0) = y''(x_0) \quad \text{and} \quad w''_F(x) < y''(x)\ (x > x_0), \tag{3}$$

in which $w_F(x)$ is the beam deflection with the curve fixture. Then, we can write the static mass displacement at the tip

$$y_m = \frac{F(L-x_0)^3}{3EI} + y(x_0) + y'(x_0)(L-x_0) \text{ in which } F = \frac{EIy''(x_0)}{L-x_0} = \frac{EI(2a_2+3a_3x_0)}{L-x_0}, \tag{4}$$

where the first term represents the contribution of the beam's deflection after the split point, the second term and the third one are accounted for the initial displacement and slope at S_0, respectively. Here, the force F are given for the case of Type 1. However, the expression of the other two types can be obtained similarly.

Eliminating x_0 in Eq. (4), we have

$$F = 2EI\left(\frac{a_2+3a_3L}{\sqrt{L^2+\frac{2a_2L^2-3y_m}{a_2+3a_3L}}} - 3a_3\right) = 2EI\left(\frac{a_2+3a_3L}{\sqrt{L^2-\frac{3(y_m-y_t)}{a_2+3a_3L}}} - 3a_3\right)\ \left(y_m > y_t = \frac{2}{3}a_2L^2\right). \tag{5}$$

Applying Taylor's expansion at $y_m = y_t$ and restricting the order to (3), we obtain

$$F = \begin{cases} \dfrac{3EI}{L^3} y_m \quad (0 < y_m < y_t) \\ \dfrac{3EI}{L^3} y_m + c_1(y_m - y_t) + c_2(y_m - y_t)^2 + c_3(y_m - y_t)^3 \quad (y_m > y_t), \end{cases} \tag{6}$$

y_t is the point corresponding to the contacting threshold F_{th} while $c_1 = F'(y_m = y_t) - 3EI/L^3$, $c_2 = F''(y_m = y_t)$, and $c_3 = F'''(y_m = y_t)$ are constant coefficients related to the device parameters. Here, Eqs. (5) and (6) only account the case of $y_m > 0$ while the expression for $y_m < 0$ can be easily obtained by symmetry.

The elastic characteristic curves of these three types of CBCF generators and the linear cantilever beam are presented in Fig. 3(a). The transition points, corresponding to y_t, which mean the CBCF generator deviating from the linear case, are also marked for each type. The generator of type 1 first behaves as a linear beam and then smoothly transits to a nonlinear generator while the type 2 directly exhibits the nonlinear properties from $y_m = 0$. Similar to type 1, the elastic curve of type 3 is composed of a linear segment and a nonlinear one, but not smooth at the transition point, which hints a sudden change of stiffness due to the immediate reduction of the beam's effective length.

With Eq. (6), the CBCF generator's dynamic equations are

$$\begin{cases} m\ddot{y}_m + \mu\dot{y}_m + F + \beta i = m\gamma(t) \\ \beta\dot{y}_m - i(R_L + r) - L_c \dfrac{di}{dt} = 0, \end{cases} \tag{7}$$

in which m is the inertial mass, μ the damping coefficient, β the electromagnetic coefficient, i the output current of the coil, r the coil resistance, L_c the inductance, R_L the load, and $\gamma(t)$ the excitation.

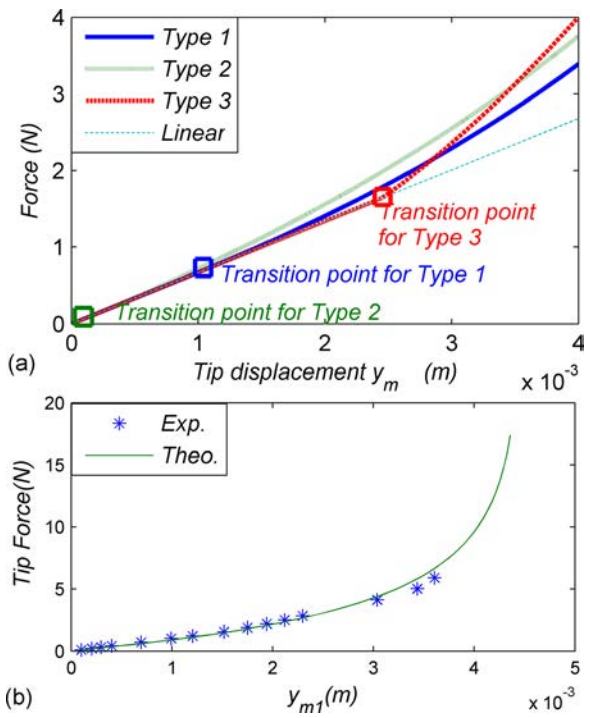

FIG. 3. Elastic curves: (a) different CBCF generators; (b) the generator prototype. Exp.: Experimental; Theo.: Theoretical.

In order to investigate the feasibility and performance of the CBCF generator, a prototype of type 1 with the shape curve $y(x) = 0.1x^2 + 5x^3$ is selected for further investigation since the studies on type 1 are applicable to type 2 directly and type 3 with special attention paid to the impact effects between the type 3 generators and the fixture due to the sudden contact. Additional damping is to be introduced while high-order issues are likely to be considered as well. The fabricated generator is presented in Fig. 1(b). It is composed of a steel cantilever beam (11 cm × 2 cm × 0.095 cm) and the curve fixture of aluminum. A permanent magnet is used as the inertial mass and also the energy converter with the coil.

Using Eq. (6) for the CBCF generator of type 1 with the curve $y(x) = a_2x^2 + a_3x^3$, we have

$$c_1 = 0 \quad c_2 = \frac{27EI}{4(a_2 + 3a_3L)L^5} \quad c_3 = \frac{405EI}{24(a_2 + 3a_3L)^2L^7}. \tag{8}$$

By substituting Eq. (6) into Eq. (7) and using Eq. (8), the final dynamic equation is then obtained. The transition point is calculated to be $y_t = 0.0008$ m with the prototype's parameters listed in Table I.

A static test is first performed to verify the prototype's elastic curve by changing the force and measuring the corresponding beam deflection. Fig. 3(b) presents both experimental and theoretical results. Good agreements are found and the linear segment of the elastic curve is clearly observed. Due to the range limitation of the laser displacement sensor (SUNX, HL-C203BE), the laser spot is placed at the position with a distance of 3 cm away from the beam tip. Therefore, the displacement at the laser spot is denoted y_{m1} (see Fig. 3(b)) to be distinguished from y_m while the theoretical results are scaled correspondingly. The same approach is applied to the followed measurements as well.

With the generator fixed on the vibrator (Dongling, ESS-26) which is driven by a signal generator (Rigol, DG1032), the device's parameters are identified through dynamic tests under open-circuit and short-circuit conditions. The mechanical quality factor Q is estimated to be 83.3 while the natural frequency of the beam is 30.3 Hz.

TABLE I. Parameters for the CBCF prototype.

Definition	Value	Definition	Value
L (m)	0.11	M (kg)	0.0197
L_F (m)	0.075	I (m^4)	1.429×10^{-12}
E (pa)	200×10^9	y_t (m)	0.0008
r (Ω)	8.1	Lc (H)	0.002
β (Wb m^{-1})	1.2	c_1	0
c_2	6.845×10^4	c_3	8.08×10^6

To investigate the wideband performance, a chirp excitation (19.6 ms^{-2}, 20 Hz–70 Hz) is applied to the CBCF device (the gravity is accounted as a constant offset here due to the vertical assembling situation). The experimental displacement and power responses are plotted in Figs. 4(a) and 4(b), respectively, in comparison with theoretical results. Both forward and reverse sweeps are performed for $R_L = 3.2\ \Omega$ and $R_L = 20.2\ \Omega$, respectively, in experiments and simulations.

A maximum power output of 165 mW at 50.8 Hz is obtained for the forward sweep with $R_L = 20.2\ \Omega$ and the half-power bandwidth is estimated to be about 8 Hz. The power density is calculated to be 2.7 mW cm^{-3} with the volume of 61.2 cm^3. As a reference, the performance of the equivalent linear generator with the same structural parameters but a regular fixture is presented in Fig. 4, showing a peak power of 196.5 mW and a bandwidth of 1 Hz around. Although the peak power of the CBCF generator is slightly worse, it has a much better bandwidth (about 8 times) with improved overall performance clearly presented. Even in the less favorable reverse case, the CBCF generator still has a peak power of 31.1 mW and a bandwidth of 3.6 Hz.

For $R_L = 3.2\ \Omega$, the power response is worse than the case of 20.2 Ω. It is partly due to the over damping from the increased current, which makes the CBCF drop from the high-energy orbit earlier. Another reason is the load mismatch with the impedance of the coil. Even in this less favorable case, a maximum power of 61.2 mW is obtained and the bandwidth of the forward sweep response is about 7 Hz. Good agreement between experiment and theory is clearly seen in Figs. 4(a) and 4(b), which validates the developed model well.

Repetitive tests are done for different load cases to acquire the load dependence properties of the generator as shown in Fig. 5. Considering the desired wideband performance, we choose to use the average power P_{av} over the tested frequency range instead of the peak power for comparison

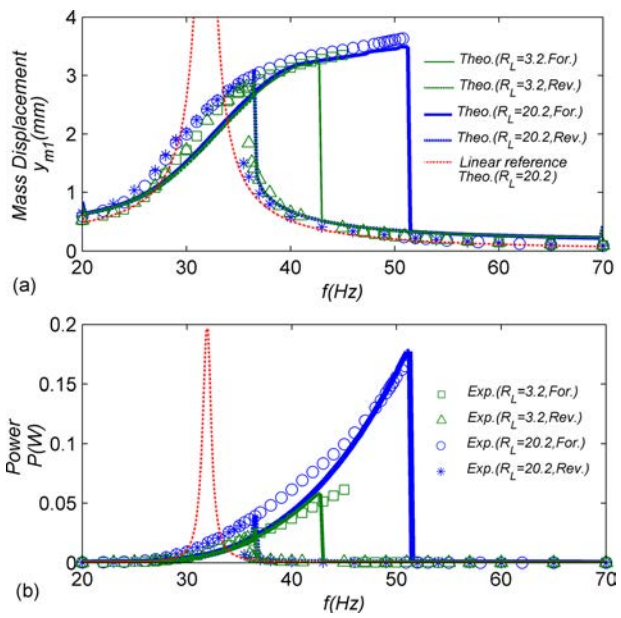

FIG. 4. Experimental and theoretical responses of the CBCF generator prototype: (a) Displacement; (b) Power. For.: Forward; Rev.: Reverse.

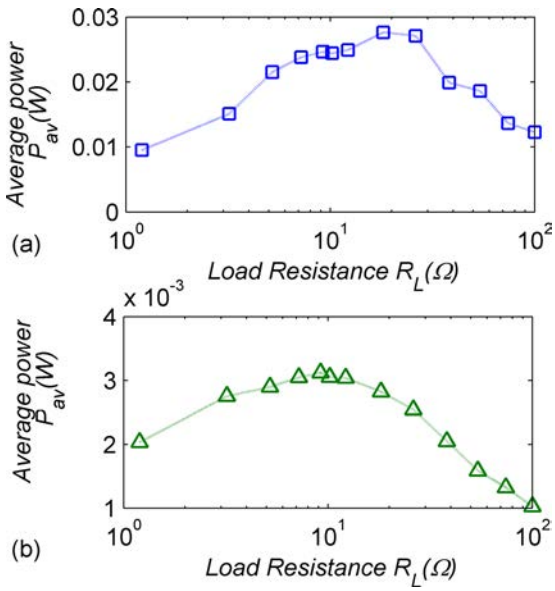

FIG. 5. Average harvested power versus load: (a) Forward sweep; (b) Reverse sweep.

$$P_{av} = \frac{1}{\omega_2 - \omega_1}\int_{\omega_1}^{\omega_2} P d\omega, \tag{9}$$

in which $\omega_1 - \omega_2$ is the concerned frequency range (20 Hz–70 Hz). By inspecting Figs. 5(a) and 5(b), the optimal load for the reverse sweep is around the internal impedance of the coil (r and L_c together) while it is higher for the forward sweep. As seen in Fig. 4, the reverse sweep responses are almost unvaried when changing the load so that the optimal performance is obtained when the load matches the internal coil impedance (around 9.2 Ω). However, the forward sweep responses are more sensitive to the load change, so that the optimal performance is achieved by letting the damping from the electric circuit match the mechanical damping with a higher load value for the sake of the prototype's high electromechanical coupling level.

In order to make comparison with the published harvesters, several FoMs (Figures of Merit), including NPD (Normalized Power Density),[30] FoM_v (volume FoM),[31] and $SFoM_{BW}$[32] (Systematic FoM with Band-Width information), are calculated for the CBCF generator as shown in Table II with some published generators. The CBCF generator presents better performance than the majority of them, especially for $SFoM_{BW}$ which is dedicated to evaluating wideband generators. Notably, some parameters of the generators in the literature are estimated from the provided response curves so that inaccuracies may exist. However, it still provides some insights about the performance of the CBCF generator.

TABLE II. Comparison between nonlinear generators.

Reference	NPD (kg s m^{-3})	FoM_v (%)	$SFoM_{BW}$ (kg m^{-3})
This work	7.02	1.1	1704.2
33	3.56	0.85	405.4
34	0.312	0.42	145.8
35	13.4	1.26	5214
21	2.21	1.43	153

In conclusion, this letter introduces a bandwidth increasing mechanism by applying a curve fixture to the cantilever generator. Investigations show that the proposed CBCF generator is capable of extending the bandwidth greatly with high power performance. The simple structure without the necessities of including pre-stress or magnetic interaction makes it feasible to apply the generator in different scales and application environments. More importantly, the design of a desired nonlinear generator becomes easy by choosing the proper fixture curve. Various configurations of the CBCF are available, which promise more choices for wideband energy harvesting. In addition, by properly arranging the magnet and the coil or using the piezoelectric material for energy conversion, the CBCF generator can be more compact with enhanced performance.

The authors would like to acknowledge the financial supports from National Natural Science Foundation of China under Grant No. 51505395 and the international cooperation project of Sichuan province under Grant No. 2016HH0028.

[1]J. A. Paradiso and T. Starner, IEEE Pervasive Comput. **4**, 18 (2005).
[2]S. P. Beeby, M. J. Tudor, and N. M. White, Meas. Sci. Technol. **17**(12), R175 (2006).
[3]S. R. Anton and H. A. Sodano, Smart Mater. Struct. **16**, R1 (2007).
[4]W. Q. Liu, A. Badel, F. Fabien, Y. P. Wu, and A. Agbossou, Smart Mater. Struct. **22**(12), 125038 (2013).
[5]D. Zhu, M. J. Tudor, and S. P. Beeby, Meas. Sci. Technol. **21**(2), 022001 (2010).
[6]L. Tang, Y. Yang, and C. K. Soh, J. Intell. Mater. Syst. Struct. **21**(18), 1867 (2010).
[7]J. Twiefel and H. Westermann, J. Intell. Mater. Syst. Struct. **24**(11), 1291–1302 (2013).
[8]V. R. Challa, M. G. Prasad, and F. T. Fisher, Smart Mater. Struct. **20**(2), 025004 (2011).
[9]L. J. Gong, Q. S. Pan, W. Li, G. Y. Yan, Y. B. Liu, and Z. H. Feng, Appl. Phys. Lett. **107**(3), 033904 (2015).
[10]Y. Tadesse and S. Priya, J. Intell. Mater. Syst. Struct. **20**(5), 625–632 (2008).
[11]P. Pillatsch, F. M. Yeatman, and A. S. Holmes, Smart Mater. Struct. **21**(11), 115018 (2012).
[12]J. Xu and J. Tang, Appl. Phys. Lett. **107**(21), 213902 (2015).
[13]Y. Zhang, K. Liu, and L. Tang, Proc. SPIE **9431**, 94310R (2015).
[14]B. P. Mann and N. D. Sims, J. Sound Vib. **319**, 515–530 (2009).
[15]S. C. Stanton, C. C. McGehee, and B. P. Mann, Appl. Phys. Lett. **95**(17), 174103 (2009).
[16]A. Hajati and S. G. Kim, Appl. Phys. Lett. **99**(8), 083105 (2011).
[17]G. Sebald, H. Kuwano, D. Guyomar, and B. Ducharne, Smart Mater. Struct. **20**(10), 102001 (2011).
[18]A. Erturk, J. Hoffmann, and D. J. Inman, Appl. Phys. Lett. **94**, 254102 (2009).
[19]F. Cottone, H. Vocca, and L. Gammaitoni, Phys. Rev. Lett. **102**(8), 080601 (2009).
[20]S. D. Nguyen, E. Halvorsen, and I. Paprotny, Appl. Phys. Lett. **102**, 023904 (2013).
[21]A. F. Arrieta, P. Hagedorn, A. Erturk, and D. J. Inman, Appl. Phys. Lett. **97**, 104102 (2010).
[22]G. Litak, M. I. Friswell, and S. Adhikari, Appl. Phys. Lett. **96**, 214103 (2010).
[23]F. Cottone, L. Gammaitoni, H. Vocca, M. Ferrari, and V. Ferrari, Smart Mater. Struct. **21**, 035021 (2012).
[24]W. Q. Liu, A. Badel, F. Formosa, Y. P. Wu, and A. Agbossou, Smart Mater. Struct. **22**(3), 035013 (2013).
[25]R. L. Harne, M. Thota, and K. W. Wang, Smart Mater. Struct. **22**(12), 125028 (2013).
[26]W. Liu, F. Formosa, A. Badel, Y. Wu, and A. Agbossou, Sens. Actuators, A **216**, 106–115 (2014).
[27]J. Cao, S. Zhou, W. Wang, and J. Lin, Appl. Phys. Lett. **106**(17), 173903 (2015).
[28]M. S. M. Soliman, E. M. Abdel-Rahman, E. F. El-Saadany, and R. R. Mansour, J. Micromech. Microeng. **18**(11), 115021 (2008).
[29]H. Liu, C. Lee, T. Kobayashi, C. J. Tay, and C. Quan, Smart Mater. Struct. **21**(3), 035005 (2012).
[30]S. P. Beeby, R. N. Torah, M. J. Tudor, P. Glynne-Jones, T. O'Donnell, C. R. Saha, and S. Roy, J. Micromech. Microeng. **17**(7), 1257–1265 (2007).
[31]P. Mitcheson, E. M. Yeatman, G. K. Rao, and T. C. Green, Proc. IEEE **96**(9), 1457–1486 (2008).
[32]W. Q. Liu, A. Badel, F. Formosa, and Y. P. Wu, Smart Mater. Struct. **24**(12), 125012 (2015).
[33]K. Ashraf, M. H. D. Khir, J. O. Dennis, and Z. Baharudin, Smart Mater. Struct. **22**(2), 025018 (2013).
[34]R. Masana and M. F. Daqaq, J. Sound Vib. **330**, 6036 (2011).
[35]W. Q. Liu, A. Badel, F. Formosa, Y. Wu, N. Bencheikh, and A. Agbossou, J. Intell. Mater. Syst. Struct. **26**, 872–877 (2015).